Int. J. Electrochem. Sci., 13 **(2018)** 29 – 44, doi: 10.20964/2018.01.36

International Journal of
ELECTROCHEMICAL
SCIENCE
www.electrochemsci.org

Evaluation of the Corrosion of AZ31 Magnesium Alloy Used as Sacrificial Anode for Cathodic Protection of Hot-Water Tank Storage Containing Chloride

N. Zidane[1], *Y. Ait Albrimi*[1], *A. Ait Addi*[1], *J. Douch*[1], *R.M. Souto*[2,3,*], *M. Hamdani*[1,*]

[1] Laboratoire d'Electrochimie, Catalyse et Environnement, Faculté des Sciences, Université Ibn Zohr, Agadir, Maroc.
[2] Department of Chemistry, Universidad de La Laguna, La Laguna (Tenerife), Spain.
[3] Institute of Material Science and Nanotechnology, Universidad de La Laguna, La Laguna (Tenerife), Spain.
[*]E-mail: rsouto@ull.es, hamdani.mohamed@gmail.com

Received: 3 July 2017 / *Accepted:* 19 September 2017 / *Online Published:* 1 December 2017

Corrosion resistance of AZ31 magnesium alloy was evaluated in aqueous chloride-containing solutions. Combined weight loss and electrochemical data indicate that corrosion rate of magnesium alloy increased for greater NaCl concentrations and higher temperatures. Corrosion is characterized by the formation of precipitates, that present the distinctive XRD patterns corresponding to crystalline phases of $Mg(OH)_2$, accompanied by H_2 evolution, these processes leading to pH increases in the solution. Retrieved samples show a film of corrosion products distributed around cracks on the bare metal surface, and the subsequent development of large pits that prevent the material from attaining passive protection.

Keywords: Corrosion; Cathodic protection; Sacrificial anode; Magnesium alloy AZ31; Potentiodynamic polarization; Electrochemical impedance spectroscopy.

1. INTRODUCTION

The corrosion of a metal in an aqueous environment is a destructive process of electrochemical origin, and accounts for big financial losses to industry. In order to avoid or reduce the impact of corrosion, cathodic protection by sacrificial anodes (SA) is often used to protect a metal against corrosion in aggressive aqueous media [1,2]. In this method, the anode is made of a material that will be corroded while the cathode is the structure to be protected from corrosion. Current will flow from the anode through the aqueous electrolyte to the cathode, and then back to the anode through the

electrical metallic contact employed to close the circuit, which facilitates the flow of electrons in the opposite direction. This procedure has the advantage that an auxiliary power supply is not required. Thus, the use of sacrificial anodes to cathodically protect a metal is a topic of interest.

The corrosion of the sacrificial anode supplies electrons to the protected metal thus hindering its natural tendency to oxidation. Corrosion occurs through the loss of metal ions at anodic areas while cathodic areas are protected from corrosion and only reduction reactions occur. However, the sacrificial anode should be adequately chosen to provide full protection of the metal whereas using cheaper and environment-friendly materials. To provide protection to a metal immersed in the water, a suitable voltage value difference is required between the sacrificial anode and the metal to be protected. Thus, the more active material used as sacrificial anode should exhibit a lower -more negative- potential to protect the cathode. Mg, Al and Zn are widely employed for this purpose, as they generate potentials of -1.50, -1.10 and -1.05 V vs. Ag/AgCl, respectively [3]. Unfortunately, magnesium-based materials often deliver rather low efficiencies as sacrificial anodes due to the combination of fast corrosion rates [4] and phenomena such as metal passivation [5], film breakdown [6], vigorous hydrogen evolution [7], chunk effects [8], and local cell action [9]. Therefore, techniques are investigated to prolong the lifetime of the Mg anode, alloying being one of the most used procedures [10]. By alloying, the mechanism of corrosion of magnesium-based materials can be changed from pitting to general corrosion [11]. The potential of the Mg alloy electrode is a mixed potential with contributions of the constituent elements according to the potential of the galvanic couple [12].Thus, when these alloying elements are added into Mg anodes, high over-potential for the hydrogen evolution reaction and large electrochemical activity are obtained [13,14]. Furthermore, alloying metals can confer high corrosion protection to magnesium by hindering its corrosion due to the formation of protective thin oxide film in its surface [15]. On the other hand, oxidation of these alloys leads to release of each individual component ions in the water (i.e. Mg^{2+}, $Al^{3+}$and Zn^{2+}), besides H_2 evolution and alkalization of the environment [16]. Accordingly, this contributes to increase the conductivity and the aggressivity of the medium [17].

Therefore, magnesium alloys are economical and attractive engineering materials for sacrificial anodes due to the combination of negative electrochemical potential and high current output per unit weight [18,19]. It has been shown that the corrosion resistance of magnesium alloys immersed in 1 M NaCl solution follows the sequence ZK60>AM60>AZ31 >AZ91 [20], whereas other report established that the corrosion resistance of AZ91 was significantly lower than that of AZ31D in simulated body fluid [21]. Feliu et al. compared the corrosion performance of AZ31 and AZ61 in 0.6 M NaCl and reported that the later was more resistant due to the formation of a thicker and more uniform oxide film on it [22,23].

The present study deals with the electrochemical corrosion behavior of an Mg alloy anode material, namely AZ31, used as sacrificial anode to protect storage tank of hot water heated by solar energy in panels installed in Morocco. In addition, magnesium sacrificial anodes are widely used in domestic water heaters throughout Morocco due to the relatively low corrosion resistance of AZ31, and sacrificial anodes of this material are currently available for corrosion protection in commercial presentations [24-26]. Since the anodic dissolution behavior of AZ31 alloy is greatly affected by the microstructure [27], grain orientation [28,29], impurity level at the surface [30], and surface treatment

or modification [31,32], more detailed studies on the corrosion performance of AZ31 are required to improve the efficiency of the material for application as sacrificial anode. In this work, electrochemical tests were conducted in NaCl solutions with concentrations 0.1, 0.5 and 1 wt.% that were chosen to simulate drinking, brine and saline waters, respectively [33,34].

2. EXPERIMENTAL

Magnesium alloy AZ31 was used in this work. The precise chemical composition was determined using inductively coupled plasma atomic emission spectroscopy (ICPAES) and is given in Table 1. Samples were cut from rods, machined into circular coupons (1.9 cm diameter and 0.5 cm thickness). The center of the magnesium rods was made of iron wire. Samples were finished by grinding all the sides with 1200 grit emery paper, washed with distilled water, degreased ultrasonically in ethanol, and finally dried in air. The entire sample was used in the weight loss measurements. For the electrochemical investigations only a quarter of this sample ($0.7 cm^2$), embedded in a glass tube using a resin (Araldite®), was employed. Sodium chloride aqueous solutions, of compositions 0.1 wt.% (1 g L^{-1}), 0.5 wt.% (5 g L^{-1}) and 1 wt.% (10 g L^{-1}), were prepared using twice-distilled water. The initial pH of the as-prepared solutions was 6.5 (± 0.1), and the temperature was kept constant using a thermo-regulated bath. The pH was measured using pH-meter (Knick 766 Calimatic). All reagents were analytical grade.

Table 1. Chemical composition of the AZ31 magnesium alloy studied in this work.

Element	Al	Zn	Mn	Fe	Pb	Mo	Cu	Bi	Mg
wt.%	3.18	1.05	0.50	0.0036	0.0072	0.0004	0.0010	0.0060	balance

After cleaning, the Mg alloy sample was immersed (in hanging position) in 200 mL of naturally aerated quiescent NaCl solutions at 20 °C. The sample was weighed before and after the immersion in the unstirred solutions in open air. The corrosion products were removed after being cleaned in 180 g L^{-1} chromic acid solution for 20 min immersion at room temperature following the procedure described elsewhere [35]. After acid cleaning, the sample was rinsed ultrasonically in ethanol, dried in the open air and then weighed. The difference in mass of the Mg-alloy sample per surface unit area is defined as the corrosion rate ($CR = \Delta m / S$), or expressed per surface unit area per time ($CR = \Delta m / (S\ t)$), where t is time (given in h) elapsed in the solution. Each measurement was performed twice on a new specimen and the average was reported. The standard deviation of the observed weight loss was less than 6%. After immersion time and before acid cleaning all specimens increased in weight. An analytical balance, with an accuracy of ±0.1 mg, was used for weighing the Mg-alloy specimens.

Electrochemical studies were carried out in the three-electrode configuration using a single-compartment glass cell. The Mg-alloy samples were connected as the working electrodes in quiescent

NaCl aqueous solution. Only one side of the specimen was in contact with the electrolyte (0.7 cm^2). The electrical contact with the opposite side of the test electrode was made using a rigid copper wire. The potential of the working electrode was measured against a saturated calomel electrode (SCE, E^0 = 0.240 V vs. SHE). The reference electrode was placed in a separate compartment, which was connected to the measuring cell through a KCl-containing agar-agar salt bridge, the tip of which was placed as close as possible to the surface of the working electrode in order to minimize the solution resistance between the test and reference electrodes (i.e., *IR* drop). The volume of the aerated and unstirred electrolyte was 200 mL. The counter electrode consisted of a platinum plate of 6 cm^2 surface area. The electrochemical characterization was performed using a potentiostat mod. Voltalab PRZ 100 (Radiometer-Analytical) under computer control.

The corrosion behaviour of the Mg-alloys was investigated using the potentiodynamic polarization technique. The polarization curves were measured after determination of the open circuit potential of the sample in the given electrolyte. For all electrochemical investigations, the open-circuit potential (OCP) was recorded for at least 30 min to ensure stabilization. The polarization curves were recorded at a scan rate of 1 mV s^{-1}. Electrochemical impedance (EIS) measurements were performed using an AC voltage amplitude of 5 mV peak-to-peak voltage excitation and a frequency range of 10^{-2}-10^5 Hz. Each experiment was performed in triplicate for reproducibility.

The chemical composition of the magnesium alloy was probed using inductively coupled plasma atomic emission spectrometry (ICPAES) analysis. A sequential type ULTIMA (Jobin Yvon Horiba) instrument was employed. Sample preparation consisted in a first cleaning step where it was rinsed ultrasonically in 2 vol.% HNO_3 acid solution, followed by metal dissolution into concentrated nitric acid.

The surface morphologies of the Mg alloy samples after corrosion testing was performed on retrieved samples using high resolution SEM (FEI QUANTA 200). For the sake of comparison, SEM analysis was also performed on non-tested samples. Analogously, eventual phase changes in the oxide layers developed on the alloy during corrosion testing were monitored by X-ray diffraction (XRD) (X'Pert PRO, PANalytical, CuKα = 1.5406 Å).

3. RESULTS AND DISCUSSION

3.1. Weight loss measurements

Weight loss measurements of AZ31 alloy immersed in 1 wt.% NaCl solution up to 48 hours are plotted in Figure 1. The weight loss, expressed in mg cm^{-2}, increased with the elapse of time. Conversely, the net corrosion rate, expressed in mg cm^{-2} h^{-1}, decreased exponentially with time at early exposures until reaching a minimum value around 15 h. Subsequently, the net corrosion rate exhibited a slow trend to increase for the remaining of the experiment, reaching the value 0.25 mg cm^{-2} h^{-1} after 48 h.

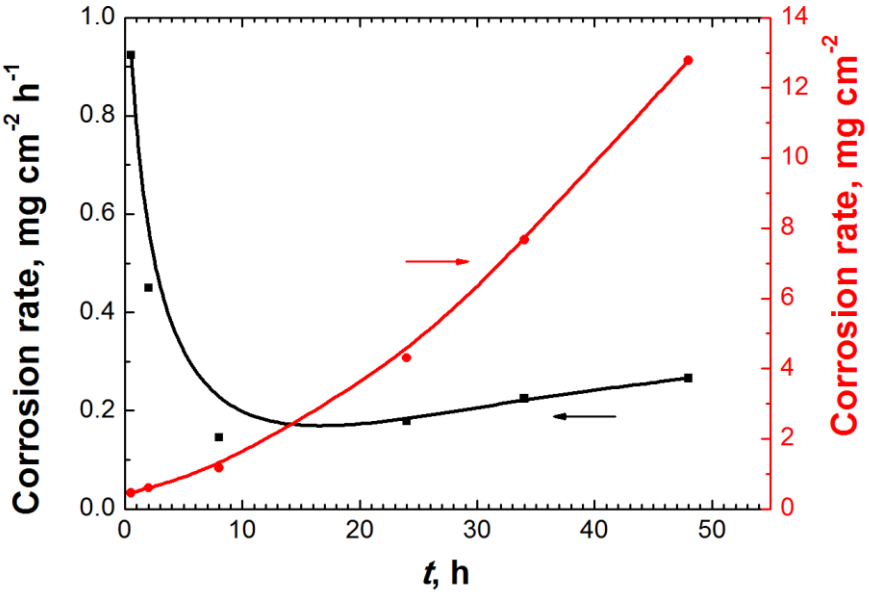

Figure 1. Weight loss of an AZ31 alloy sample in 1 wt.% NaCl solution as a function of immersion time.

Monitoring of solution pH during immersion tests was performed. Figure 2 shows its time evolution following immersion of a Mg sample in 1 wt.% NaCl at 20 °C. Shortly after immersion, the pH increased sharply during the first 20 min, and then progressively tended to a steady state condition around pH = 10.5 that was reached around 30 min immersion. The final value of pH was found to be the same regardless the concentration of the test solution. The dissolution of a magnesium anode in aqueous solutions proceeds by the reduction of water to produce magnesium hydroxide and hydrogen gas evolution reaction on the cathodic sites [36]. This pH increase arises from the increase of OH^- concentration by production of hydroxyl ions in the solution. Magnesium dissolution occurred in anodic half-cell (reaction 1), whereas water reduction accompanied by hydrogen evolution occurred in the cathodic process (reaction 2), these reactions being mostly insensitive to oxygen concentration in chloride-containing neutral and alkaline environments [37-40]:

$$Mg \rightarrow Mg^{2+} + 2e^- \quad (1)$$

$$2H_2O + 2e^- \rightarrow H_2 + 2OH^- \quad (2)$$

The combined effect of the cathodic and anodic half-cell reactions produces corrosion of magnesium and hydrogen generation. It must be noticed that some authors consider that Mg^+ species is involved in the corrosion mechanism of pure magnesium and Mg alloys in chloride media in order to explain the hydrogen evolution that takes place under anodic polarization [41-44]. Yet there is no definite experimental evidence of its occurrence [45-50], and therefore it was not considered here due to its very likely instability in aqueous solution [51].

The occurrence of a plateau in Figure 2 can be justified on the basis of a report by Song and Atrens [38] where the increasing corrosion resistance of magnesium alloys in alkaline solutions when pH exceed 10.5 was attributed to the pH of a saturated $Mg(OH)_2$ with formation of $Mg(OH)_2$ film on the magnesium surface. Therefore, it is proposed that the decrease of the corrosion rate observed in this work must be related to the formation of a $Mg(OH)_2$ film on the surface of the corroding material.

Figure 3 shows weight loss after 2 h immersion in 1 wt.% NaCl solution determined at various temperatures, namely at 20, 30, 40, 50 and 60 °C. At 20 °C, the weight loss was about 0.4 mg cm^{-2} h^{-1}, and this corrosion rate doubled by raising 20 degrees the temperature of the solution.

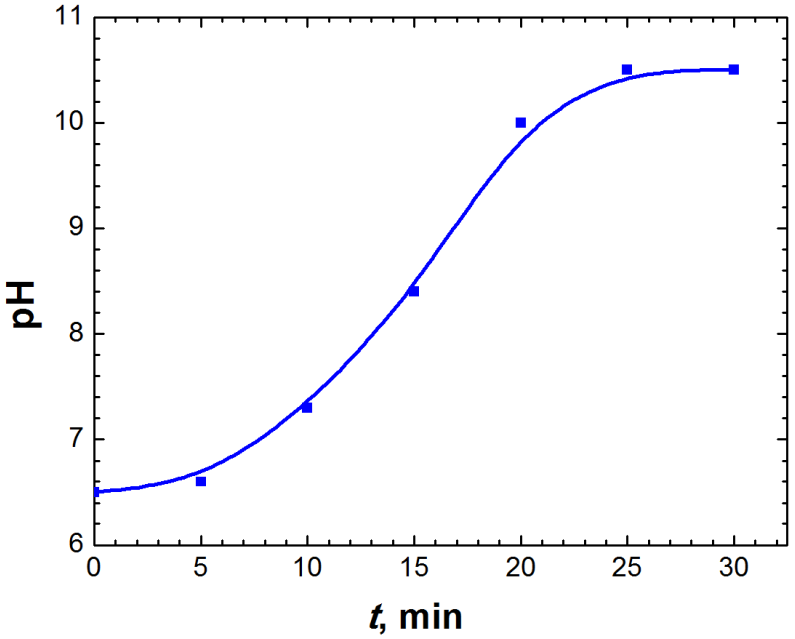

Figure 2. pH variation in the solution pH during immersion of an AZ31 alloy sample in 1 wt.% NaCl solution as a function of time.

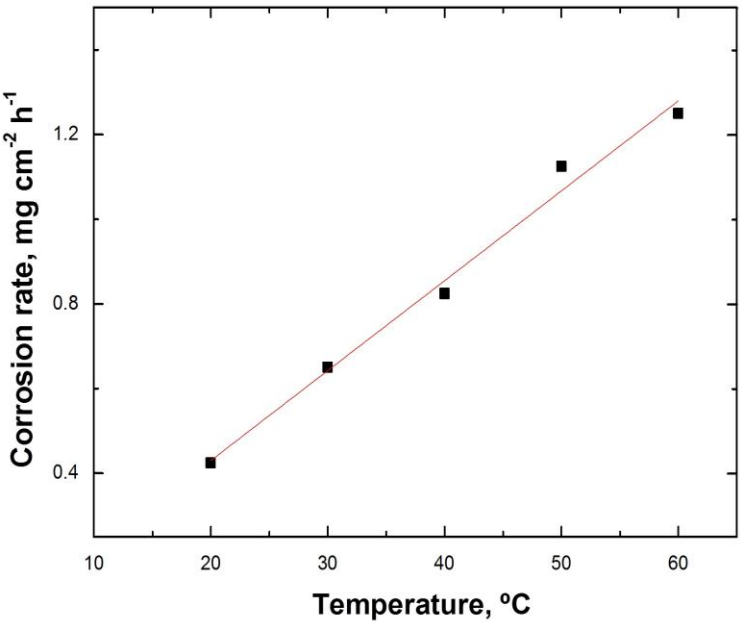

Figure 3. Effect of temperature on the weight loss of an AZ31 alloy sample in 1 wt.% NaCl solution.

The data derived from weight loss measurements were also used to estimate the average corrosion resistance of the alloy, and it was expressed in mm year^{-1} according to the following equation [35]:

$$CR = \frac{8.76 \times 10^4}{A \times t \times \rho} \Delta m \quad (3)$$

where Δm is the weight change (in g), A is the surface area (in cm^2), t is the immersion time (in h), and ρ is the density of the alloy (in g cm^{-3}). In this work, the density of magnesium alloys AZ31 was taken to be 1.754 g cm^{-3} [35,52]. Accordingly, the calculated corrosion rates were 46.1, 22.5, 7.3, 9.0, 11.2 and 13.3 mm year^{-1} after respectively 0.5, 2, 8, 24, 34 and 48 h immersion in 1 wt.% NaCl at 20 °C. In addition, the corrosion rate increased with increasing temperature delivering 21.3, 32.5, 41.3, 56.3 and 62.5 mm year^{-1} respectively for 20, 30, 40, 50 and 60 °C exposure to the same electrolyte during 2 h.

3.2. Electrochemical measurements

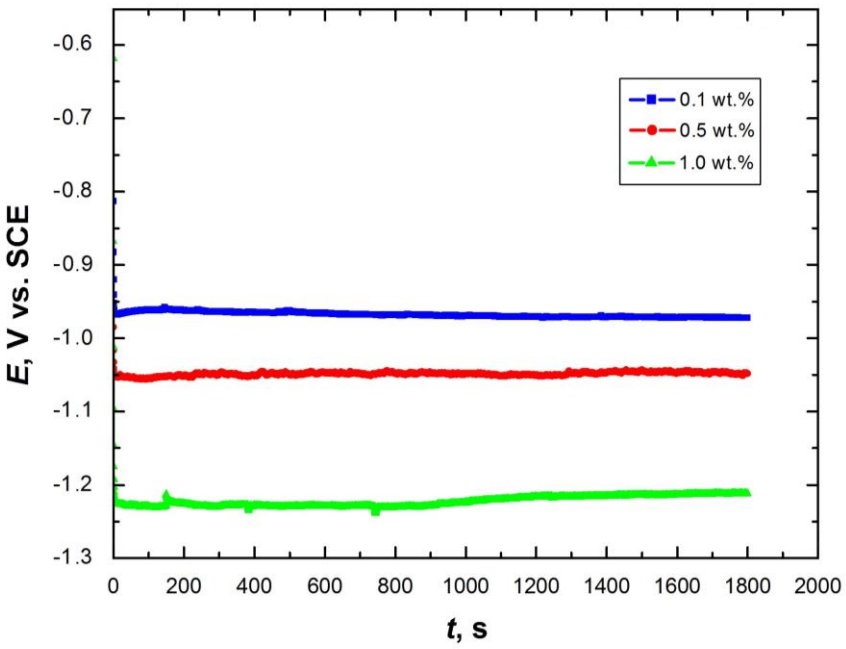

Figure 4. Open circuit potential (OCP) of AZ31 alloy during immersion for 30 min in 0.1 (blue), 0.5 (red) and 1 (green) wt.% NaCl at 20 ºC.

The time evolution of the open circuit potential, E_{oc}, of the magnesium alloy was monitored for 30 min in the various test solutions of different NaCl concentration considered in this work, and it is given in Figure 4. A transient behavior was only observed at the beginning of the experiment, extending for about 20-30 s, consisting in an abrupt shift towards more negative (less noble) values, followed by a rather prolonged almost stationary behaviour. Therefore, it was regarded that sufficient stabilization of the alloy electrical condition could be ensured by elapsing 30 min since immersion, for the electrochemical measurements to be recorded. Table 2 lists the experimentally found E_{oc} values

referred to the saturated calomel electrode. It can be observed that E_{oc} values strongly depended on the concentration of the solution. E_{oc} values shifted in the negative direction with increasing salt concentration. This feature evidences that AZ31 presents a greater driving force towards corrosion with increasing NaCl concentration.

Table 2. Relevant electrochemical parameters of AZ31 immersed in NaCl solutions of various concentrations at 20 ºC derived from potentiodynamic polarization curves.

NaCl concentration, wt.%	E_{oc}, V vs. SCE	E_{cor}, V vs. SCE	j_{cor}, µA cm^{-2}	$-\beta_c$, mV decade^{-1}	β_a, mV decade^{-1}
0.1	-0.967	-1.061	1.986	-324	314
0.5	-1.048	-1.099	4.977	-366	457
1.0	-1.212	-1.285	13.611	-313	507

The corrosion behaviour of the magnesium alloy was subsequently investigated using the potentiodynamic polarization technique. Polarization measurements were performed to gain knowledge concerning the kinetics of the cathodic and anodic reactions. The polarization tests were conducted at various salt concentrations, namely 0.1, 0.5 and 1 wt.% NaCl solutions, in order to envisage the effect of chloride concentration. Figure 5 depicts typical potentiodynamic polarization curves of the magnesium alloy electrode, registered after 30 min immersion in the electrolyte at 20 °C. The potential of the working electrode was swept, at 1 mV s^{-1} scan rate, from -0.800 V to +0.800 V with respect to the corresponding open circuit corrosion potential of the sample in the electrolyte. The plots exhibited a rather symmetrical curve around the corrosion potential, revealing that the metal was in its active state. Table 2 gives the relevant electrochemical parameters extracted by Tafel analysis of the graphs, namely the corrosion potential (E_{cor}), the corrosion current density (j_{cor}), and the cathodic and anodic Tafel slopes ($-\beta_c$ and β_a, respectively). The corrosion current densities I_{cor} obtained by extrapolation of the Tafel lines allowed estimation of the corrosion rates in the various electrolytes, giving approximately 2×10^{-6}, 5×10^{-6}, and 13.6×10^{-6} A cm^{-2} in 0.1, 0.5, and 1 wt.% NaCl solutions. It is evident that the current densities increased whereas the corrosion potentials decreased with increasing salt concentration. The cathodic Tafel slopes remained almost the same regardless the composition changes, a feature indicating the cathodic process remained invariant. The cathodic branches of the plots were almost parallel, with a Tafel slope of ca. 0.35 V decade^{-1}, corresponding to the simultaneous reduction of oxygen and water. Conversely, the anodic Tafel slopes increased with the electrolyte concentration.

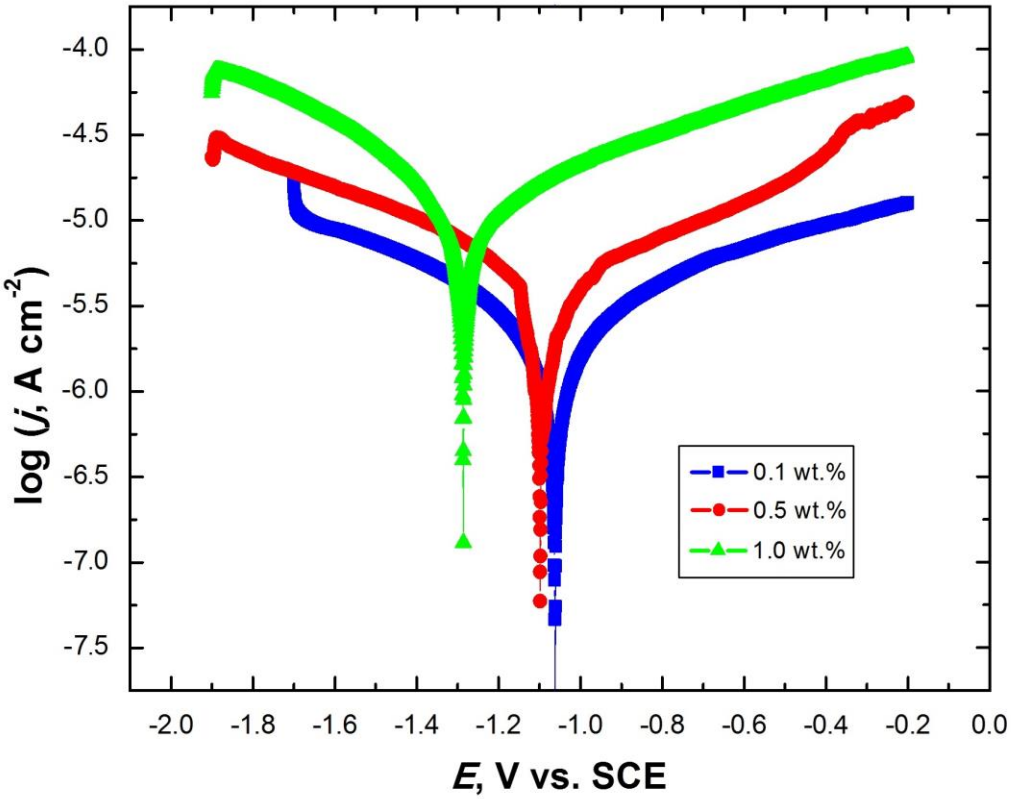

Figure 5. Potentiodynamic polarization curves of AZ31 alloy in 0.1 (blue), 0.5 (red) and 1 (green) wt.% NaCl at 20 ºC; v = 1 mV s^{-1}.

The corrosion behavior of AZ31 alloy was also investigated by electrochemical impedance spectroscopy (EIS) after 30 min immersion in the same solutions and experimental conditions. EIS data were plotted in the form of Nyquist (complex versus real components of the impedance) and Bode (impedance modulus and phase angle versus frequency) diagrams in Figure 6. Nyquist representation showed depressed semicircles in the tested solution concentrations. The depression in Nyquist semicircle is often observed for solid electrodes, and frequency dispersion is attributed to roughness and inhomogeneities of the electrode surface. The radius of the depressed semicircle, which mostly corresponded to the impedance for frequency values tending to zero, decreased when the NaCl concentration increased. This parameter was directly proportional to the corrosion resistance of the magnesium alloy in the given salt solution. Though the occurrence of a second time constant in the spectra became observable in the case of the most concentrated NaCl solution of 1 wt.% during inspection of the Nyquist plots (cf. Figure 6A), the corresponding Bode diagrams given in Figure 6B-C evidenced both two time constants were present in the other less concentrated solutions too. That is, two electrochemical processes competitively operated in the system, one directly related to the dissolving metal/electrolyte interface, and the second corresponding to the formation of a partially blocking oxide layer on the surface of the material. The latter had to be highly inhomogeneous and porous in order to account for the rather big depression angles of the Nyquist arcs.

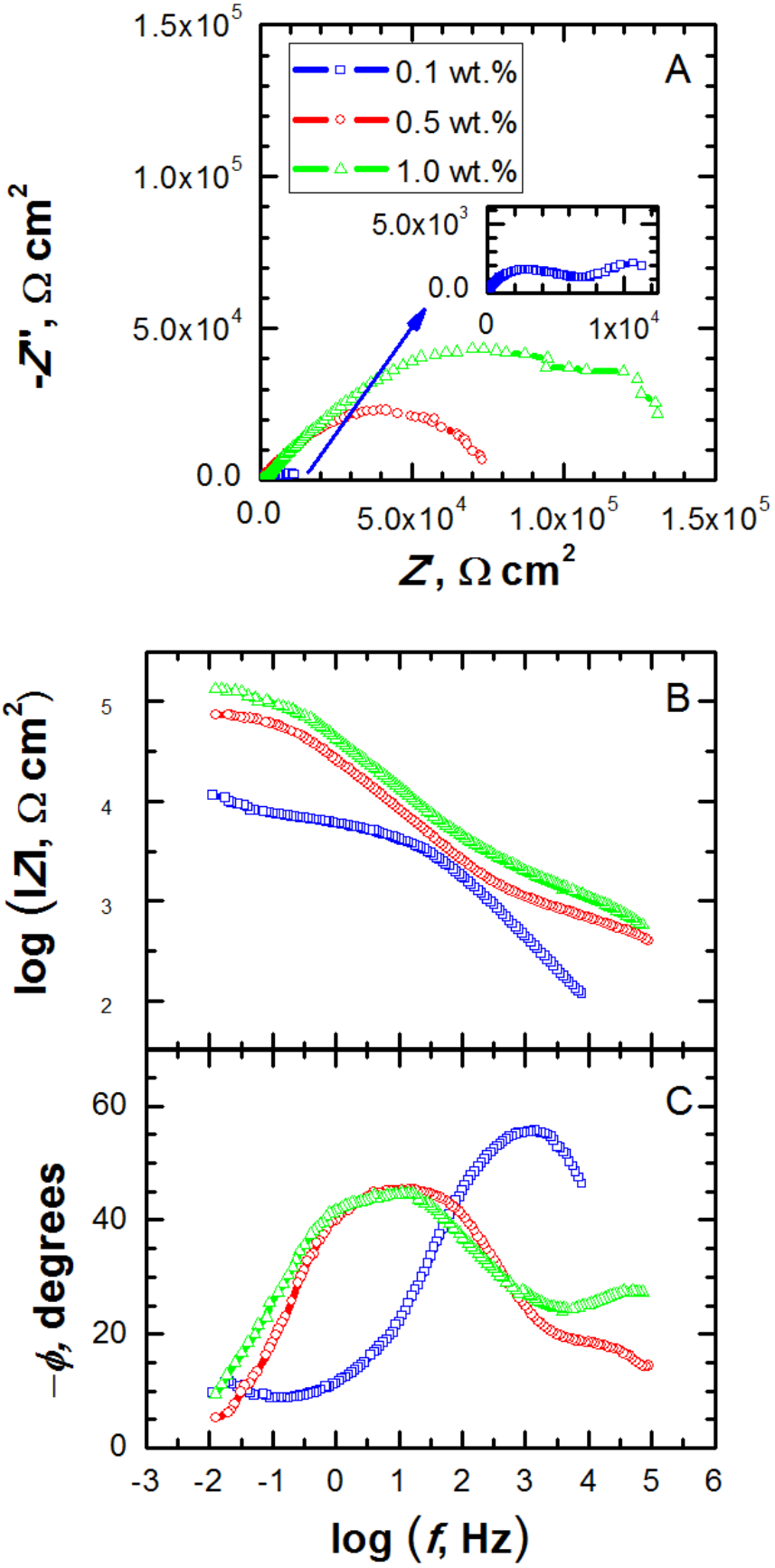

Figure 6. Measured (discrete points) and fitted (solid lines) impedance spectra of AZ31 alloy in 0.1 (blue), 0.5 (red) and 1 (green) wt.% NaCl at 20 ºC.

In order to describe the corrosion resistance of the system from EIS data, the equivalent circuit (EC) in Figure 7 was considered. This EC was previously employed by Shanab et al. to describe the impedance spectra recorded for AZ31E in artificial sea water (namely, 3.5 wt.% NaCl), although they used capacitors and resistors exclusively [53]. A better fit was obtained this time by using constant phase elements (CPE) instead of pure capacitances [54,55], because they accounted for the non-ideal capacitive response determined by the distributed relaxation feature of the oxide films formed on the metallic materials. The same procedure was employed by Sherif for magnesium in natural seawater and 3.5 wt.% NaCl solutions [56]. The rather good agreement between experimental and fitted data is observed in Figure 6, where the discrepancies between both data sets were almost exclusively confined to the low frequency limit. Since longer times were required to collect a single data point, they were thus more sensitive to the dynamic surface changes occurring on the actively corroding magnesium alloy. Despite these limitations, this equivalent circuit was regarded to provide sufficiently satisfactory description of the frequency-dependence of the impedance, and the extracted parameters are listed in Table 3. R_{sol} accounts for the ohmic loss in the solution for the current flow between the magnesium alloy sample and the auxiliary electrode, which is greatly affected by the conductivity changes related to the different ionic content. The time constant occurring at higher frequencies accounts for the characteristics of the metal/electrolyte interface, namely the charge transfer resistance R_1 in parallel to the double layer capacity Q_1. In addition, the second time constant (R_2Q_2) is related to the formation of a porous barrier-defective surface layer on the material [42]. The corrosion of magnesium, in this case, probably forms a thick film of $Mg(OH)_2$ which partially hinders the transport of aggressive chloride anions and water through this surface layer. The low diffusivity of the Cl^- ions through the film originates a straight line at low frequencies which forms a 45º angle with respect to the *X* axis in the Bode-magnitude diagrams of Figure 6B.

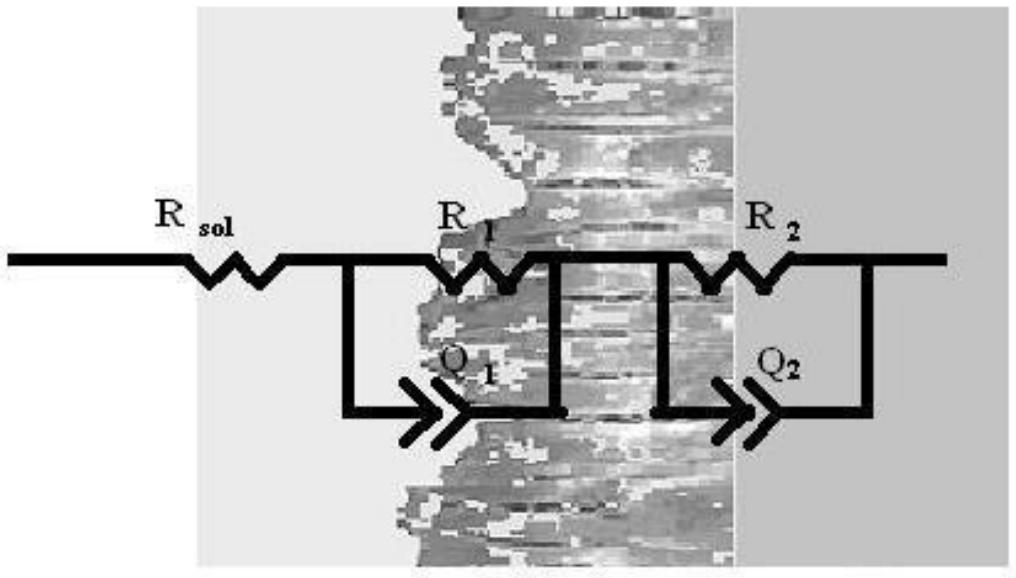

Figure 7. Equivalent circuit (EC) used to model the impedance data.

Table 3. EIS-fitted results of AZ31 magnesium alloy immersed in NaCl solutions of various concentrations at 20 ºC. AC polarization was applied around their corresponding open circuit potential values in the electrolytes.

NaCl concentration, wt.%	R_{sol}, Ω cm^2	Q_1, μS cm^{-2} s^n	n_1	R_1, kΩ cm^2	Q_2, μS cm^{-2} s^n	n_2	R_2, kΩ cm^2
0.1	524	6.7	0.59	161	4.4	0.46	1.5
0.5	252	9.7	0.60	84.5	1.0	0.68	0.40
1.0	25	5.7	0.70	5.2	333	0.50	8.2

The formation of an oxide-based surface layer on the corroding AZ31 magnesium alloy upon exposure to NaCl aqueous solution was confirmed by X-ray diffraction characterization of the retrieved samples. Figure 8 shows the diffractograms of samples retrieved after different exposure durations in the test electrolyte. For the sake of comparison, the diffractogram of an unexposed AZ31 sample is also given. It can be seen that only one unambiguous peak occurred at 2θ = 34.5° for the unexposed material. This signal arose from the magnesium present in the alloy matrix, whereas the remaining features were very weak and could be hardly distinguished above the background signal in the XRD pattern of Mg alloy sample.

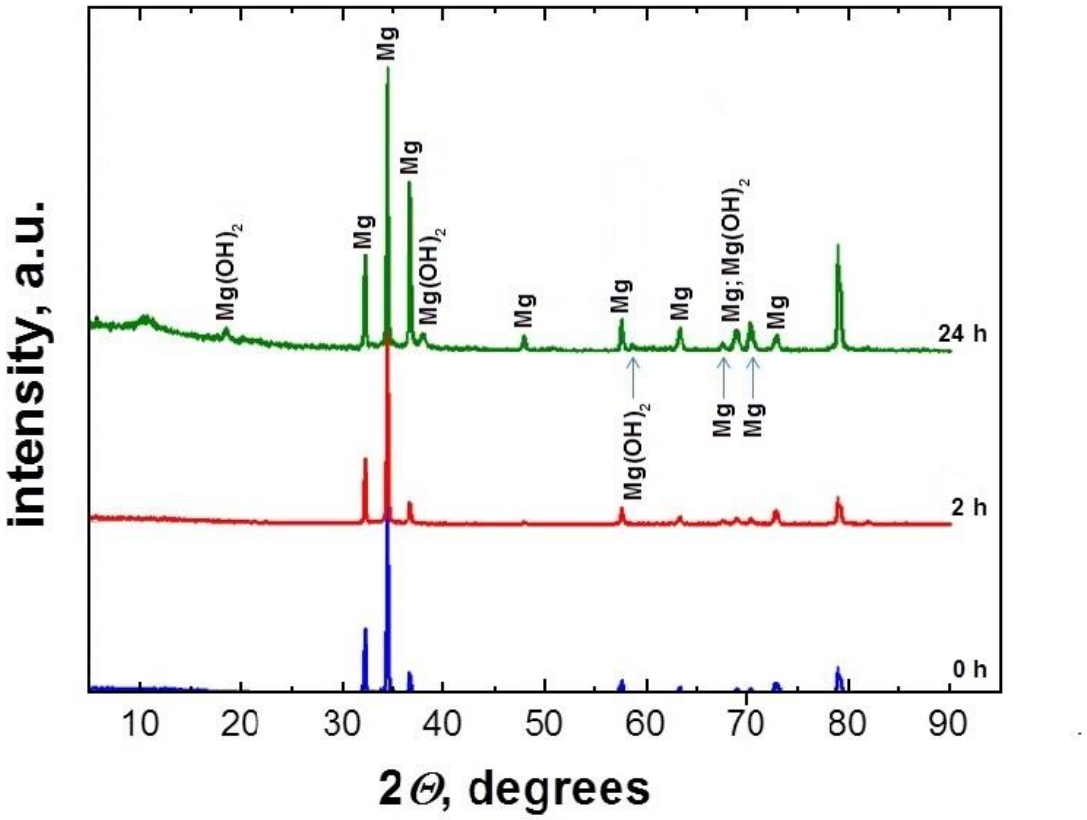

Figure 8. X-ray diffraction patterns of non-exposed and retrieved AZ31 alloy samples in 1 wt.% NaCl at 20 ºC. Immersion times in the test solution are indicated in the graph.

The X-ray diffractogram of the retrieved samples did not show any relevant $Mg(OH)_2$ patterns after 2 h immersion in 1 wt.% NaCl solution, but they were clearly distinguishable for longer exposures up to 24 h. This fact can be assigned to the different time scales required for metal dissolution and subsequent precipitation of the formed hydroxide, thus implying a certain induction time. Alternately, the lack of $Mg(OH)_2$ signals in the diffractogram of the sample exposed for a shorter time could be due to either poor crystallinity of the deposit, or more possibly because the oxide surface film only partially covered the corroded sample [57]. On the other hand, when the immersion time was extended up to 24 h, $Mg(OH)_2$ patterns appeared due to the formation of hydroxide film on the AZ31 magnesium alloy, though no specific MgO patterns were found. Therefore, the protective film formed on AZ31 in NaCl environments was mainly constituted by $Mg(OH)_2$, in good agreement with other reports [38].

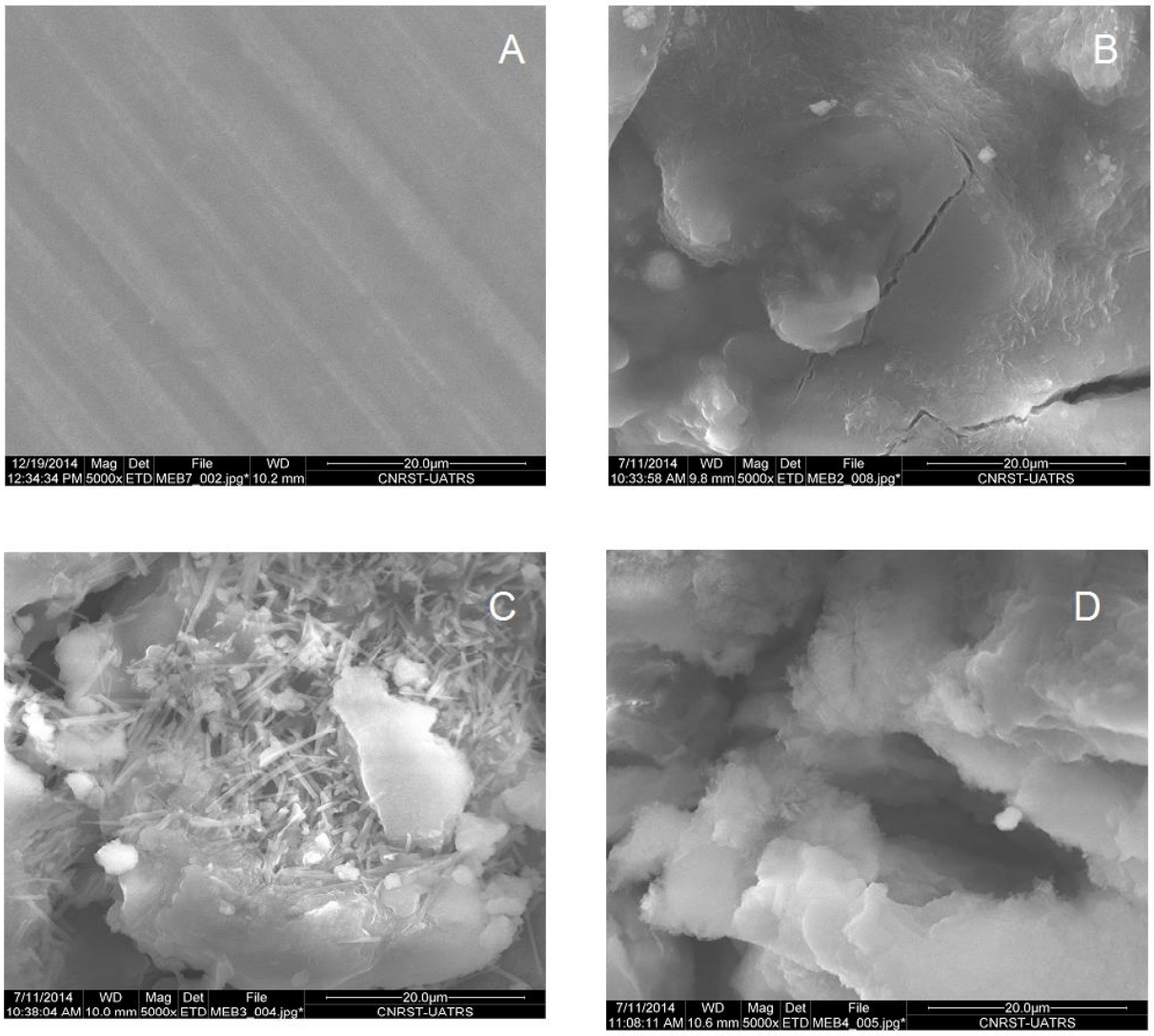

Figure 9. SEM micrographs of non-exposed and retrieved AZ31 alloy samples in 1 wt.% NaCl at 20 ºC. Immersion time: (A) 0, (B) 2, (C) 24, and (D) 48 h.

The formation of a precipitated surface film on the corroding magnesium alloy even at the shorter times covered during the electrochemical characterization, was demonstrated by SEM characterization of the surface morphology of the retrieved samples. Figure 9 shows the effect of exposure length on the topography of the samples tested in 1 wt.% NaCl at 20 ºC, together with the morphology of an unexposed sample. The samples exhibited different morphologies following immersion in the chloride-containing solution. The progressive deposition of greater amounts of precipitates with the elapsed time in the test electrolyte was then evidenced. Whereas the unexposed magnesium alloy surface presented a rather smooth surface only evidencing the predominant direction of grinding stages on the material, the morphology of the alloy after immersion for only 2 h in the chloride solution demonstrated the presence of corrosion products in granular shape deposited on the smoother metal substrate, though presenting the development of cracks. The image obtained after 24 h immersion showed the agglomeration of corrosion deposits on the metal surface, presenting needle-shaped aggregates of 10 µm approximate length. Longer exposure for 48 h showed corrosion product precipitates covering the complete surface of the alloy, with the deposits adopting a 3D cotton-like texture. They were deposited around deep pits penetrating the underlying metal surface.

4. CONCLUSIONS

AZ31 magnesium alloy was immersed in NaCl aqueous solutions at 20 ºC of various concentrations in order to ascertain its electrochemical behavior in environments simulating drinking, brine and sea waters. Despite major changes in the observed corrosion resistance of the material resulting from the different aggressivity of the test aqueous electrolytes, it has been evidenced that metal dissolution was eventually accompanied by precipitation reactions leading to the formation of a porous surface layer mainly composed by $Mg(OH)_2$. This surface layer was not able to protect the metal from further corrosive attack, though it might eventually decrease the corrosion rate for longer exposures. Corrosion rates of the material in the various environments were successfully determined from the combination of weight loss and electrochemical measurements, and physicochemical observations were adequately supported by SEM and XRD characterization of retrieved samples after exposure.

ACKNOWLEDGEMENTS

SEM and XRD analysis at the CNRST/UTARS unit in Rabat, and ICPAES measurements at Marrakech University are acknowledged. R.M.S. acknowledges financial support by the Spanish Ministry of Economy and Competitiveness (MINECO, Madrid) and the European Regional Development Fund, under grant CTQ2016-80522-P.

References

1. W. Von Baeckmann, W.S. Schwenk and W. Prinz, Handbook of Cathodic Corrosion Protection, 3rd edn. Gulf Professional Publishing, Houston, TX, 1997.

2. M.R. Saeri and A. Keyvani, *J. Mater. Sci. Technol.*, 27 (2011)785.
3. M. Narozny, K. Zakowski and K. Darowicki, *Corros. Sci.*, 88 (2014) 275.
4. G.-L. Song, in: G.-L. Song (Ed.), Corrosion of Magnesium Alloys, Woodhead Publishing Limited, Cambridge, UK, 2011, Ch. 1.
5. G.-L. Song, K.A. Unocic, H. Meyer III, E. Cakmak, M.P. Brady, P.E. Gannon, P. Himmer and Q. Andrews, *Corros. Sci.*, 104 (2016) 36.
6. G.R. Hoey and M. Cohen, *J. Electrochem. Soc.*, 105 (1958) 245.
7. G.-L. Song and K.A. Unocic, *Corros. Sci.*, 98 (2015) 758.
8. C.D. Lee, C.S. Kang and K.S. Shin, *Met. Mater. Int.*, 7 (2001) 385.
9. J.I. Skar, *Mater. Corros.*, 50 (1999) 2.
10. B.L. Mordike and T. Ebert, *Mater. Sci. Eng. A*, 302 (2001) 37.
11. R. Zeng, K.U. Kainer, C. Blawert and W. Dietzel, *J. Alloy Compd.*, 509 (2011) 4462.
12. Y. Feng, R.-C. Wang and C.-Q. Peng, *T. Nonferr. Metals Soc.*, 23 (2013) 2650.
13. K.W. Guo, *Recent Pat. Corros. Sci.*, 2(2010) 13.
14. S.R. Shamsudin, A. Rahmat, M. Che Isa, M.N. Derman and A.R. Daud, *Adv. Mater. Res.*, 795 (2013) 530.
15. L. Liu, R. Xu, and G. Song, *Surf. Coat. Technol.*, 205 (2010) 332.
16. A. Kiss, R.M. Souto and G. Nagy, *Period. Polytech. Chem. Eng.*, 57 (2013) 11.
17. M.S. Jellesen, D. Minzari, U. Rathinavelu, P. Møller, R. Ambat, *ECS Trans.*, 25 (30) (2010) 1.
18. J.G. Kim, J.H. Joo and S.J. Koo, *J. Mater. Sci. Lett.*, 19 (2000) 477.
19. B.-L. Yu and J.-Y. Uan, *Scripta Mater.*, 54 (2006) 1253.
20. Y.-L. Cheng, T.-W. Qin, H.-M. Wang and Z. Zhang, *T. Nonferr. Metals Soc.*, 19 (2009) 517.
21. Z. Wen, S. Duan, C. Dai, F. Yang and F. Zhang, *Int. J. Electrochem. Sci.*, 9 (2014) 7846.
22. S. Feliu Jr., C. Maffiotte, A Samaniego, J.C. Galván and V. Barranco, *Appl. Surf. Sci.*, 257 (2011) 8558.
23. S. Feliu Jr., A. Samaniego, V. Barranco, A.A. El-Hadad, I. Llorente and P. Adeva, *Corros. Sci.*, 80 (2014) 461.
24. Made-in-China.com, http://fr.made-in-china.com/tag_search_product/sacrifical-anode_ugouoshn_1.html (last accessed on June 10, 2017).
25. Corroco International Industrial Co., http://www.cathodic-protection.net/fr/Magnesium-Anode-products.html (last accessed on June 10, 2017).
26. Anode de magnésium pour chauffe eau. https://french.alibaba.com/g/magnesium-anode-rod-for-water-heater.html (last accessed on June 10, 2017).
27. G.-L. Song and Z.Q. Xu, *Electrochim. Acta*, 55 (2010) 4148.
28. Z. Pu, G.-L. Song, S. Yang, J.C. Outeiro, O.W. Dillon Jr., D.A. Puleo and I.S. Jawahir, *Corros. Sci.*, 57 (2012) 192.
29. G.-L. Song, *J. Mater.*, 64(2012) 671-679.
30. G.-L. Song and Z. Xu, *Corros. Sci.*, 54 (2012) 97.
31. Y. Choi, S. Salman, K. Kuroda and M. Okido, *Corros. Sci.*, 63 (2012) 5.
32. G.-L. Song and M. Liu, *Corros. Sci.*, 62 (2012) 61.
33. http://bv.alloprof.qc.ca/science-et-technologie/la-terre-et-l%27espace/les-caracteristiques-generales-de-la-terre/l%27hydrosphere/la-salinite-de-l%27eau.aspx. La salinité de l'eau.(last accessed on June 10, 2017).
34. http://hydrologie.org/glu/FRDIC/DICSALEE.HTM. Eau(x) salée(s). (last accessed on June 10, 2017).
35. N. Hort, Y. Huanga, D. Fechner, M. Störmer, C. Blawert, F. Witte, C. Vogt, H. Drücker, R. Willumeit, K.U. Kainer and F. Feyerabend, *Acta Biomater.*, 6 (2010) 1714.
36. R. Ambat, N.N. Aung and W. Zhou, *J. Appl. Electrochem.*, 30 (2000) 865.
37. H.H. Uhlig and R.W. Revie, Corrosion and Corrosion Control, John Wiley and Sons, New York, 1985, Ch. 20.

38. G.L. Song and A. Atrens, *Adv. Mater. Res.*, 1 (1999) 11-33.
39. S. Thomas, N.V. Medhekar, G.S. Frankel and N. Birbilis, *Curr. Opin. Solid St. M.*, 19 (2015) 85.
40. Z. Shi, J.X. Jia and A. Atrens, *Corros. Sci.*, 60 (2012) 296.
41. R.I. Petty, A.W. Davidson and J. Kleinberg, *J. Am. Chem. Soc.*, 76 (1954) 363.
42. Y. Song, D. Shan, R. Chen, F. Zhang and E.-H. Han, *Mater. Sci. Eng. C*, 29 (2009) 1039.
43. W. Bai, J. Yu, Y. Yang, Y. Ye, J. Guo and Y. Zhang, *Int. J. Electrochem. Sci.*, 8 (2013) 3441.
44. A. Atrens, G.-L. Song, M. Liu, Z. Shi, F. Cao and S.S. Dargusch, *Adv. Mater. Res.*, 17 (2015) 400.
45. G. Williams and H.N. McMurray, *J. Electrochem. Soc.*, 155 (2008) C340.
46. N.T. Kirkland, G. Williams and N. Birbilis, *Corros. Sci.*, 65 (2012) 5.
47. J. Izquierdo, L. Nagy, I. Bitter, R.M. Souto and G. Nagy, *Electrochim. Acta*, 87 (2013) 283.
48. G. Williams, H. ap Ll. Dafydd and R. Grace, *Electrochim. Acta*, 109 (2013) 489.
49. S. Lebouil, A. Duboin, F. Monti, P. Tabeling, P. Volovitch and K. Ogle, *Electrochim. Acta*, 124 (2014) 176.
50. A.D. King, N. Birbilis and J.R. Scully, *Electrochim. Acta*, 121 (2014) 394.
51. A.C. Harms, S.N. Khanna, A.B. Chen and A.W. Castleman, *J. Chem. Phys.*, 100 (1994) 3540.
52. S. Lee, H.J. Ham, S.Y. Kwon, S.W. Kim and C.M. Suh, *Int. J. Thermophys.*, 34 (2013) 2343.
53. S.M.M. Shanab, M.A. Ameer, A.M. Fekry, A.A. Ghoneim and E.A. Shalaby, *Int. J. Electrochem. Sci.*, 6 (2011) 3017.
54. J. R. Macdonald, *Solid State Ionics* 13 (1984) 147.
55. D. Mareci, L.C. Trinca, V.V. Cotea and R.M. Souto, *Int. J. Electrochem. Sci.*, 12 (2017) 5438.
56. E.-S.M. Sherif, *Int. J. Electrochem. Sci.*, 7 (2012) 4235.
57. S.S. Pathak, S.K. Mendon, M.D. Blanton and J.W. Rawlins, *Metals*, 2 (2012) 353.